



Seasonal variation of atmospheric particle number concentrations, new particle formation and atmospheric oxidation capacity at the high Arctic site Villum Research Station, Station Nord

Quynh T. Nguyen^{1,2,3}, Marianne Glasius^{2,4,6}, Lise L. Sørensen^{1,6}, Bjarne Jensen¹, Henrik Skov^{1,5,6}, Wolfram Birmili⁷, Alfred Wiedensohler⁷, Adam Kristensson⁸, Jacob K. Nøjgaard¹, and Andreas Massling^{1,6}

¹Department of Environmental Science, Aarhus University, 4000 Roskilde, Denmark

²Department of Chemistry, Aarhus University, 8000 Aarhus, Denmark

³Department of Engineering, Aarhus University, 8200 Aarhus, Denmark

⁴Interdisciplinary Nanoscience Center (iNANO), Aarhus University, 8000 Aarhus, Denmark

⁵Institute of Chemical Engineering and Biotechnology and Environmental Technology, University of Southern Denmark, 5230 Odense, Denmark

⁶Arctic Research Centre, Aarhus University, 8000 Aarhus, Denmark

⁷Leibniz Institute for Tropospheric Research, 04318 Leipzig, Germany

⁸Department of Physics, Lund University, P.O. Box 118, 221 00 Lund, Sweden

Correspondence to: Quynh T. Nguyen (quynh@eng.au.dk)

Received: 9 March 2016 – Published in Atmos. Chem. Phys. Discuss.: 15 March 2016

Revised: 20 June 2016 – Accepted: 18 August 2016 – Published: 13 September 2016

Abstract. This work presents an analysis of the physical properties of sub-micrometer aerosol particles measured at the high Arctic site Villum Research Station, Station Nord (VRS), northeast Greenland, between July 2010 and February 2013. The study focuses on particle number concentrations, particle number size distributions and the occurrence of new particle formation (NPF) events and their seasonality in the high Arctic, where observations and characterization of such aerosol particle properties and corresponding events are rare and understanding of related processes is lacking.

A clear accumulation mode was observed during the darker months from October until mid-May, which became considerably more pronounced during the prominent Arctic haze months from March to mid-May. In contrast, nucleation- and Aitken-mode particles were predominantly observed during the summer months. Analysis of wind direction and wind speed indicated possible contributions of marine sources from the easterly side of the station to the observed summertime particle number concentrations, while southwesterly to westerly winds dominated during the darker months. NPF events lasting from hours to days were mostly observed from June until August, with fewer events ob-

served during the months with less sunlight, i.e., March, April, September and October. The results tend to indicate that ozone (O₃) might be weakly anti-correlated with particle number concentrations of the nucleation-mode range (10–30 nm) in almost half of the NPF events, while no positive correlation was observed. Calculations of air mass back trajectories using the Hybrid Single Particle Lagrangian Integrated Trajectory (HYSPPLIT) model for the NPF event days suggested that the onset or interruption of events could possibly be explained by changes in air mass origin. A map of event occurrence probability was computed, indicating that southerly air masses from over the Greenland Sea were more likely linked to those events.

1 Introduction

Climate change driven by anthropogenic greenhouse gas emissions is a global challenge. In the Arctic, the warming climate has already led to an earlier onset of spring-ice melt, later freeze-up and decreasing sea-ice extent (Zwally et al., 2002; Markus et al., 2009; Stroeve et al., 2012). The reduc-

tion of the Earth's albedo due to ice loss subsequently impacts the radiative balance of the Earth through a positive feedback, leading to further warming. As a result, the Arctic has been considered a manifestation of global warming with the rate of temperature increase in the region being twice as high as the rest of the world (IPCC, 2013; ACIA, 2005), up to 8–9 °C along the east coast of Greenland (Stendel et al., 2008). In addition to long-lived greenhouse gases, short-lived climate forcers including tropospheric ozone, aerosols and black carbon also play a significant role in affecting the radiative balance in the Arctic (Quinn et al., 2008; Bond et al., 2013; IPCC, 2013).

Aerosol particles influence the radiative balance in the Arctic in many ways, through their ability to absorb and scatter incoming solar radiation or by acting as cloud condensation nuclei to form cloud and fog droplets. The presence of low-level liquid clouds above bright ice- and snow-covered surfaces in the Arctic could lead to increasing near-surface temperature as opposed to a cooling effect observed in most other global regions (Shupe and Intrieri, 2004; Bennartz et al., 2013), though the effect is probably small (AMAP, 2011). At the same time, deposition of black carbon on Arctic snow- and ice-covered surfaces accelerates surface heating and ice melting in early spring (Hansen and Nazarenko, 2004; Flanner et al., 2007, 2009). It is thus crucial to investigate the dynamics of atmospheric aerosol particles observed in the Arctic (involving the formation, concentration, physico-chemical properties, temporal variability and transport) to understand their direct and indirect effects on the radiation budget.

It is well known that during each winter extending into spring, Arctic aerosol particles containing mineral dust, black carbon, heavy metals, elements and sulfur and nitrogen compounds are detected in elevated concentrations. This has been attributed to the annually recurring Arctic haze phenomenon, which is related to distant latitude anthropogenic pollution (Li and Barrie, 1993; Quinn et al., 2002; Ström et al., 2003; Heidam et al., 2004, 1999; Nguyen et al., 2013). The focus was thus on long-range transported aerosols, which are expected to be aged due to the long transport distance from midlatitude source regions.

A number of studies have reported in situ formation of new aerosol particles in the Arctic, which mostly involved new particle formation in the Arctic boundary layer. The first observations of the occurrence of an ultrafine particle mode (< 20 nm) in the Arctic marine boundary layer during summer and autumn were reported by Wiedensohler et al. (1996) and Covert et al. (1996). Observations of small aerosol particles during the summer period have also been reported at the Zeppelin mountain site, Svalbard (11.9° E, 78.9° N; 478 m a.s.l.), within the Arctic boundary layer (Ström et al., 2003; Tunved et al., 2013). The current understanding on mechanisms of new particle formation in the marine boundary layer over the Arctic Ocean is unclear, due to the low concentration of nucleating agents such as sulfuric acid in the

marine boundary layer (Pirjola et al., 2000; Karl et al., 2012), in addition to the limited number of observational data. Growth of ultrafine particles has been observed at Summit, Greenland (38.4° W, 72.6° N; 3200 m a.s.l.) (Ziemba et al., 2010). Quinn et al. (2002) also found an increase in particle number concentrations during the summer months at Barrow, Alaska (156.6° W, 71.3° N; 8 m a.s.l.), which was attributed to the formation of smaller particles. A correlation between summertime particle number concentrations and the biogenic production of methane sulfonate (MSA⁻) was shown, indicating that the production of summertime particles may be associated with biogenic sulfur (Quinn et al., 2002). A similar finding has recently been reported by Leaitch et al. (2013) based on observations from Alert, Nunavut. Heintzenberg et al. (2015) observed newly formed small aerosol particles during several cruises to the summer central Arctic Ocean and suggested that they could originate from around the Arctic region, more specifically related to air masses passing by open waters prior to the observation point. Asmi et al. (2016) also recently suggested that new particle formation (NPF) was more common in marine air masses compared to continental air flows. Meanwhile, source regions of aerosol particles in the Arctic could be very different (Hirdman et al., 2010). Barrow is mostly influenced by North America and the Arctic Basin with some Russian and Siberian sources (Quinn et al., 2002). Summit, which is located above the planetary boundary layer, receives frequent long-range transported pollution from North America and extensively from Eurasia during wintertime (Kahl et al., 1997; Hirdman et al., 2010). The mountainous site Zeppelin (Tunved et al., 2013) and the ground-level site Villum Research Station, Station Nord (VRS) (16°40' W, 81°36' N; 30 m a.s.l.) (Heidam et al., 2004; Nguyen et al., 2013), both receive long-range transported pollution predominantly from Eurasia during winter and spring. Zeppelin is often located south of the polar front, receiving transport from the Atlantic Ocean during summer (Tunved et al., 2013). Svalbard is also influenced by the Gulf Stream (Pnyushkov et al., 2013) and surrounded by open sea during summertime. VRS is influenced by the ice stream from the Arctic Ocean along the east coast of Greenland (Stendel et al., 2008; Kwok, 2009) and surrounded by multi-year sea ice, with limited first-year ice along the coast. Such differences could have considerable impacts on NPF events and also aerosol particle properties, which require investigations at high spatial resolution in the Arctic.

VRS, Station Nord is a unique coastal station located close to sea level, representing the conditions of the high Arctic throughout the year. To date, there is only one observation and characterization of NPF events at Alert, Nunavut (Leaitch et al., 2013). Understanding of particle size distribution and seasonality, as well as related mechanisms and processes of NPF events, are thus lacking from the high Arctic region.

This study aims to characterize the formation, concentration, physical properties and seasonality of atmospheric

aerosols based on particle number size distributions at VRS. The occurrence of NPF events was investigated in detail. The events were classified and analyzed together with ozone (O_3) and nitrogen oxides ($NO_x = NO + NO_2$). Wind direction and wind speed were analyzed to investigate the impacts of source regions on the observed seasonality of particle number size distribution. The source regions of new particle formation were mapped based on calculations of air mass back trajectories using the HYSPLIT model during event days and non-event days. A probability map for NPF event occurrence was computed.

2 Methods

2.1 Measurement site

Aerosol particles and trace gases were measured at the measurement site “Flyger’s Hut”, VRS, Station Nord, in northeast Greenland ($81^{\circ}36' N$, $16^{\circ}40' W$; 30 m a.s.l.). The site is located on a small peninsula (Princess Ingeborg Peninsula) at approximately 2.5 km southeast of a small Danish military base housing a crew of five soldiers (Fig. 1). Electricity at Flyger’s Hut is supplied from a local JET A-1 fuel generator located inside the military base. The remote location of the station implies a minor, though unavoidable, contribution of local anthropogenic pollution originating from the military camp. The station is surrounded by multiyear sea ice, with limited bare ground occasionally and limited first-year ice along the coast of Greenland during the summer months. At VRS, Station Nord, polar sunrise is observed at the end of February, while polar day prevails from mid-April to the beginning of September and polar night prevails from mid-October to the end of February.

2.2 Instrumentation

2.2.1 Mobility Particle Size Spectrometer

Measurement of particle number size distributions at Station Nord was initiated in July 2010 using a TROPOS-type Mobility Particle Size Spectrometer as described in Wiedensohler et al. (2012). Briefly, the instrument consists of a medium Vienna-type Differential Mobility Analyzer (DMA) followed by a butanol-based Condensation Particle Counter (CPC 3772 by TSI Inc., Shoreview, USA). The DMA design is described in Winklmayr et al. (1991). The system is operated at $1 L min^{-1}$ aerosol flow rate and $5 L min^{-1}$ sheath air flow rate. The DMA sheath flow is circulated in closed loop, facilitated by a regulated air blower. This technical setup allows measurements across a particle size range from 10 to 900 nm in diameter. The time resolution of the instrument is 5 min, including up-scan and down-scan.

The instrument was specifically designed to allow long-term operation with minimum maintenance as follows. The DMA sheath air flow rate was continuously measured using

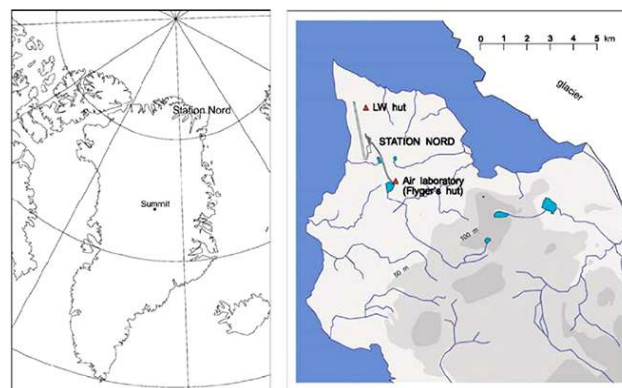


Figure 1. The high Arctic site Villum Research Station, Station Nord ($81^{\circ}36' N$, $16^{\circ}40' W$; 30 m a.s.l.), in northeast Greenland. The main measurement site is Flyger’s hut, which is located about 2.5 km southeast of the Danish military base.

a calibrated mass flow sensor. The DMA aerosol flow rate was monitored by a pressure drop measurement over a calibrated capillary. A computer-based control program adjusted the sheath air flow rate after each measurement of the particle number size distribution. Systematic deviations in the sample flow rate, which was controlled by a critical orifice in the CPC, were monitored and corrected for in the successive size distribution evaluation. Additionally, absolute pressure was measured at the inlet of the system to detect any substantial technical problems such as clogging of the inlet. Temperature and relative humidity (RH) were monitored at several positions inside the instrument. The RH inside the DMA is the most critical parameter, since excessive moisture would allow particles to grow much beyond their nominal dry diameter. At VRS, Station Nord, RH is usually not a critical issue, as the climate is cold and arid with low humidity most of the year. The temperature in the laboratory is mostly considerably higher than outdoor temperature, implying that substantial drying of the aerosol is not needed most of the time during sample intake into the laboratory.

Sampling was provided from a conductive flow tube. An air blower was used to suck a main air flow (much higher than the sample flow) into the main sampling inlet, and the air sampling was probed from this main air flow using a 1/4 inch tube directed into the main air flow. The main sampling inlet was not heated; however, no icing issue was observed for the inlet. The main sampling inlet did not have any size cut-off. Sampling was performed at standard conditions of about $20^{\circ}C$.

2.2.2 Data processing

The raw particle electrical mobility distributions collected by the Mobility Particle Size Spectrometer were processed by a linear inversion algorithm presented in Pfeifer et al. (2014). A specific DMA transfer function was used for inverting the

data, while CPC efficiency and diffusion losses were corrected for during the inversion.

As a first part of quality control, any data associated with DMA excess air RH above 50 % and sheath air temperature above 30 °C were excluded from further data analysis, as recommended by ACTRIS and WMO-GAW (<http://www.wmo-gaw-wcc-aerosol-physics.org/recommendations.html>). These incidents were only observed on a few days during the study period.

Subsequently, daily particle number size distributions were plotted to inspect any sudden increase in the particle number concentration above the background. If such sudden increase in particle number concentration (without any detectable particle growth) coincided with sudden elevation of NO_x concentration, they were interpreted as local pollution events and excluded from the data set. These local pollution events were observed throughout the year at the station. Figure 2 shows the extent of data coverage over the study period. Gaps in the data set (most notably in 2011) were due to excluded data with flow uncertainties. 2012 was the year with the best data coverage, with the lowest percentage of ca. 78 % in March, while it exceeded 90 % in most other months. The year 2012 was therefore chosen to examine the seasonality of Arctic aerosols in detail. Data from the other years were used to support the analysis of event statistics. Details of the data period used are provided in the caption of the relevant tables or figures.

2.2.3 Gas phase and meteorological parameters

O₃ was measured using an API (Advanced Pollution Instrumentation) photometric O₃ analyzer (M400). The results were averaged to a time resolution of 30 min. The detection limit was 1 ppbv, with an uncertainty of 3 and 6 % for measured concentrations above and below 10 ppbv, respectively. The uncertainties were calculated at 95 % confidence interval.

NO_x was averaged to a time resolution of 30 min (Teledyne API M200AU, San Diego, CA), with a precision of 5 % and a detection limit of 150 ppt. The calibration was checked weekly using 345 ppb NO span gas, while zero gas was added each 25 h. NO_x was sampled at a flow rate of 1 L min⁻¹. Coverage of O₃ and NO_x data in this study is indicated as the corresponding blue and red lines in Fig. 2.

Wind speed and wind direction data were obtained from a sonic anemometer (METEK, USA-1, heated) for the period from April 2011 to April 2013. The sonic is placed on a horizontal boom at the top of a 9 m mast. The mast is situated about 36 m east-southeast from the measurement hut at ca. 62 m a.s.l. This means that the fetch-limited wind direction is 300° where the hut (2.8 m) is an obstacle. The area is flat for 10–20 km in all wind directions. In winter periods fewer data were obtained due to frost on the anemometer when temperature was below approximately −35 °C.

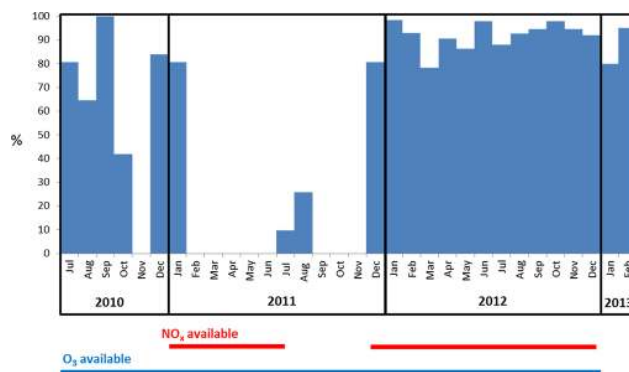


Figure 2. SMPS, O₃ and NO_x data coverage at Station Nord from July 2010 to February 2013.

2.3 Classification of new particle formation events

NPF events were identified and classified following a scheme adapted from Dal Maso et al. (2005). A brief description is given here.

A plot was compiled for each day with available particle number size distribution data, plotting the particle diameter on the y axis, and time of the day (from midnight to midnight) on the x axis, with the particle number concentration in each size interval displayed as a contour plot. A panel of three persons performed visual inspection, identification and classification of data to avoid subjective bias. In order to be classified as an event day, the occurrence of a new particle mode below 20 nm with concentrations substantially higher than during the previous hours must be observed. If a clear diameter growth of newly formed particles could be traced for several hours, that specific day would be classified as a class I event day. If the growth of newly formed particles was not continuous over several hours, that specific day would be classified as a class II event day. The identified NPF events at Station Nord typically lasted from hours to days. In the case of a multi-day event, only the first day, during which the event onset was identified, was counted as an event day. The panel must agree on all classifications, otherwise the specific day would be classified as an undefined event. Other options for classifications are “non-event day” or “bad data” in the case of missing data or observed instrumental problems.

3 Results and discussion

This section presents the observed overall seasonality of particle number size distributions measured at VRS, Station Nord, during the time period from July 2010 to February 2013, with an analysis of NPF event cases together with the atmospheric oxidation capacity at the station. Analysis of local wind speed, wind direction and air mass back trajectories was used to support the interpretation of the seasonal-

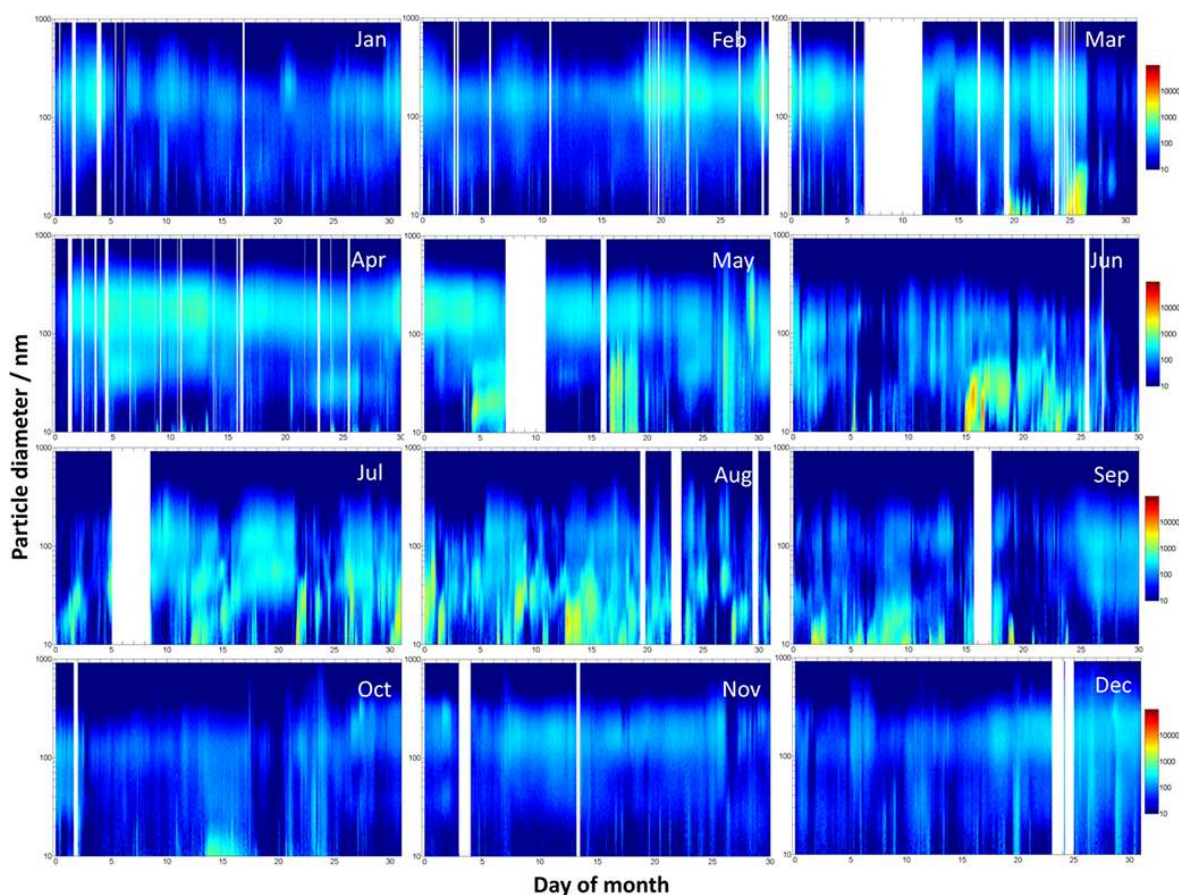


Figure 3. Time series of particle number size distributions as $dN/d\log D_p$ (cm^{-3}) during 2012. The original 5 min time resolution was used in the plots.

ity of particle number size distributions and the dynamics of NPF events.

3.1 Particle number size distributions and seasonality

3.1.1 Overview

A clear seasonality of particle number size distributions was observed during 2012 (Figs. 3–4). A persistent accumulation mode appeared at the end of September, which became more prominent at the end of February lasting until mid-May. The Arctic summer (June–August) was coupled with a higher abundance of nucleation-mode and Aitken-mode aerosol particles and a very low abundance of accumulation-mode particles (Table 1). The small particles were also observed to a lesser extent in September and only during one episode in mid-October. This observation of strong seasonality was supported by observations from the available scattered data in the other years 2010, 2011 and 2013. The elevated concentrations of accumulation-mode particles observed in this study generally followed the varying pattern of aged total suspended particles during the Arctic haze period previously reported at VRS, Station Nord (Heidam et al., 2004; Nguyen

et al., 2013), and other Arctic stations (Quinn et al., 2002; Ström et al., 2003). It should also be noted that the sun rises at the end of February at Station Nord, so the period thereafter is affected by photochemical processes. Observations of smaller particles during this period were in accordance with previous studies in the Arctic (Ström et al., 2003; Tunved et al., 2013; Wiedensohler et al., 1996; Covert et al., 1996; Quinn et al., 2002; Heintzenberg et al., 2015; Leaitch et al., 2013). During this period, the Arctic is considerably cleaner with respect to long-range transport of atmospheric pollutants and is characterized by constant daylight.

3.1.2 Statistics of the particle number size distributions

Figure 4 and Table 1 describe detailed statistics of the particle number size distributions measured at the site, showing the prominent accumulation mode during February–May and the prominent nucleation/Aitken mode during June–August. Table 2 provides detailed median and average particle number concentration (N), particle volume concentration (V) and particle mass concentration (M) values calculated using the particle number size distributions at VRS, Station Nord, during 2012. Higher values of median or average N

Table 1. Three modes were fitted to the average monthly data of 2012 using log-normal fitting. The parameters shown for each mode include the modal number concentration (N , cm^{-3}), the modal geometrical mean diameter (D_g , nm) and the modal geometrical standard deviation (GSD). A fitted sum of three log-normal distributions was calculated for the entire particle size range (averaged monthly particle number size distributions), and the difference of the sum of the squares of each number concentration at the specific sizes between the real and the fitted data was minimized using the Excel solver add-in.

	N_1 (cm^{-3})	$D_{g,1}$ (nm)	GSD ₁	N_2 (cm^{-3})	$D_{g,2}$ (nm)	GSD ₂	N_3 (cm^{-3})	$D_{g,3}$ (nm)	GSD ₃
January	5	22	1.4	72	68	3.3	50	167	1.6
February	22	27	2.2	58	97	2.7	75	169	1.5
March	24	17	1.7	49	84	2.8	93	179	1.7
April	45	24	2.4	38	48	1.6	172	167	1.6
May	17	18	1.2	134	43	2.5	125	173	1.5
June	252	17	1.9	22	31	1.4	45	113	1.5
July	196	21	2.6	24	45	1.3	50	119	1.6
August	287	16	2.3	51	30	1.5	49	114	1.8
September	90	11	1.5	25	29	1.4	57	107	1.8
October	25	9	1.3	60	41	3.3	24	139	1.5
November	12	16	1.7	45	62	2.6	51	173	1.5
December	31	22	2.4	48	100	2.5	35	170	1.5

Table 2. Median and average particle number concentration (N), particle volume concentration (V) and particle mass concentration (M) for the 12 months of 2012. M was calculated from V , assuming a density of 1.4 g cm^{-3} and particle sphericity.

	Median N (cm^{-3})	Average N (cm^{-3})	Median V ($\mu\text{m}^3 \text{ cm}^{-3}$)	Average V ($\mu\text{m}^3 \text{ cm}^{-3}$)	Median M ($\mu\text{g m}^{-3}$)	Average M ($\mu\text{g m}^{-3}$)
January	104	121	0.44	0.69	0.61	0.96
February	123	149	0.69	0.82	0.97	1.15
March	170	174	1.10	1.13	1.54	1.58
April	231	253	0.88	0.93	1.24	1.30
May	221	268	0.78	0.78	1.09	1.09
June	137	277	0.14	0.15	0.20	0.21
July	229	237	0.17	0.20	0.23	0.29
August	227	313	0.19	0.21	0.27	0.29
September	124	137	0.18	0.18	0.25	0.25
October	71	87	0.17	0.25	0.24	0.35
November	96	100	0.40	0.42	0.55	0.59
December	85	107	0.30	0.57	0.42	0.80

were observed from April to September. During this period, largest discrepancies between the median and the average values were also found, especially during June (median $N = 137$ particles cm^{-3} , average $N = 277$ particles cm^{-3}) and August (median $N = 227$ particles cm^{-3} , average $N = 313$ particles cm^{-3}). This was attributed to the occurrence of intense NPF events during these months (Fig. 3), skewing the average N towards higher values compared to median N . June and August also showed highest average N in 2012, followed by May, April and July, whereas the months with the lowest average N were October, November and December.

Newly formed particles are usually high in number and therefore significantly influence the total number concentration N as discussed above; however, they do not contribute

considerably to the total particle volume concentration V . As a result, June and August were among the months with the lowest median or average V together with other sunlit months, i.e., July and September (Table 2). In contrast, the highest median and average V values were observed during the most prominent haze months, March–May. Simple log-normal fitting applied to the accumulation mode observed in the monthly particle number size distributions in 2012 revealed a geometrical mean diameter of approximately 170 nm during the winter and spring months (Table 1). This indicates that the particles can originate from distant locations due to their longer lifetimes determined by their size (Massling et al., 2015).

The total particle mass concentrations M were derived directly from the total particle volume concentration V , assum-

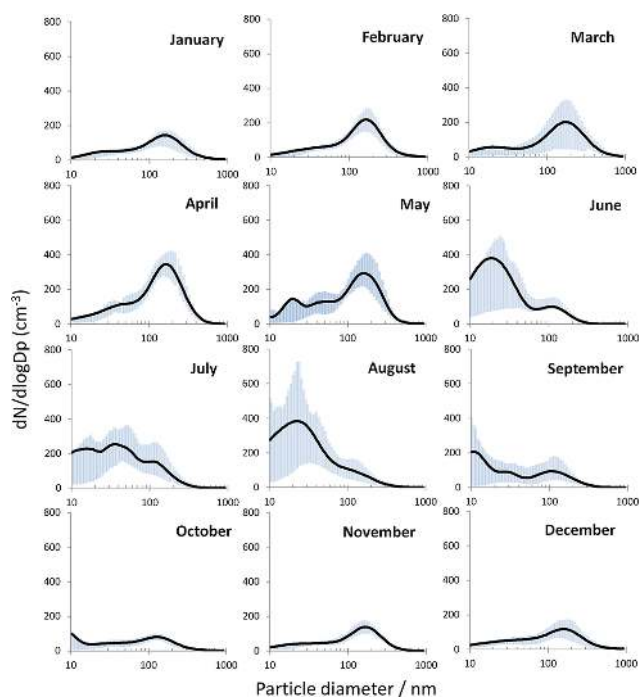


Figure 4. Monthly median particle number size distribution at Station Nord during 2012. The corresponding log-normal fitting parameters are shown in Table 1. The shade area shows the 75th (upper) and 25th (lower) percentile of the actual data.

ing a density of 1.4 g cm^{-3} and particle sphericity. Average monthly estimates of M ranged from $0.21 \mu\text{g m}^{-3}$ (June) to $1.58 \mu\text{g m}^{-3}$ (March) (Table 2).

Similar distribution of the major modes was also observed at the Zeppelin mountain site by Tunved et al. (2013). However, the nucleation mode and Aitken mode observed during the summer months seemed considerably more pronounced at VRS, Station Nord, compared to Zeppelin. This indicates higher number concentrations of smaller particles at Station Nord, which were visible until October (Figs. 3–4). In regard to the total particle mass concentration, Tunved et al. (2013) reported summer M mostly below $0.2 \mu\text{g m}^{-3}$ and higher M below $0.8 \mu\text{g m}^{-3}$ observed at Zeppelin during the prominent haze months, March–April (with an assumed lower density of 1 g cm^{-3}). Clearly, the particle mass concentration at Villum Research Station (VRS), Station Nord, seemed comparable during summer, while showing higher concentrations during the Arctic haze months compared to Zeppelin, with different assumed particle densities already accounted for. This difference between the two sites could be partially attributed to their different locations as discussed above. In addition, the study periods and lengths of the studies were also different, as the Zeppelin data were averaged for March 2000–March 2010, whereas the descriptive distribution statistics in this work was derived solely from data in 2012. Nevertheless, similar observations at both stations

show the consistent and predictable annual behavior of the particle number size distributions in the Arctic.

3.1.3 Impacts of seasonal wind pattern

Analysis of wind direction and wind speed was performed to investigate the impacts of wind pattern on the particle number size distributions at the station. Figure 5 demonstrates monthly wind roses during 2012, where two distinct patterns could be identified during the darker (September–April) and the summer (June–August) periods. The early haze months (January and February) and the prominent haze months (March and April) showed prevailing wind arriving from the southwesterly to westerly direction. During May, some northerly wind was observed, while the frequency of southwesterly wind seemed to decrease. During the summer period (June–August), when smaller and freshly formed particles were observed, easterly wind became more prominent, especially during July and August. September marked a prompt change in the wind direction back to a southwesterly direction. The wind speed became higher during November–December, which is probably due to increasing katabatic winds from the ice sheet. During the other years, 2011 and 2013 (data not shown), considerably similar patterns were observed for the corresponding months.

Earlier studies on source apportionment of total suspended particles observed during the Arctic haze period at VRS mostly identified Siberian industries and long-range transport from midlatitudes as major factors (Nguyen et al., 2013; Heidam et al., 2004). However, the wind pattern shown here may indicate an immediate impact of the adjacent southwesterly to westerly regions contributing to the properties of particles prior to arrival at the station.

Based on the summer wind pattern, the smaller particles observed during June–August were probably linked to sources from the easterly side of the station, with some marine contribution. During summer, the marine contribution from the easterly direction is possibly driven by the retreat of sea-ice cover, which exposes areas of open waters (“open leads”) and meltwater on top of sea ice to wind stress, especially along the coastline of Greenland due to the presence of first-year ice in these regions. This would result in enhanced primary emissions of sea spray particles (Korhonen et al., 2008). Surface active organic species in the ocean surface layer, which are more abundant due to increased biological activity during summer, could also be released into the atmosphere by bubble bursting (Middlebrook et al., 1998; Tervahattu et al., 2002) and become mixed with other sea spray particles. It was suggested by Sellegri et al. (2006) that this could also alter the number size distributions of particles. Another study by Karl et al. (2013) proposed that new nanoparticles in the high Arctic could be marine granular nanogels injected into the atmosphere from evaporating cloud droplets. Recent analysis of particle number size distributions and back trajectories during summer cruises

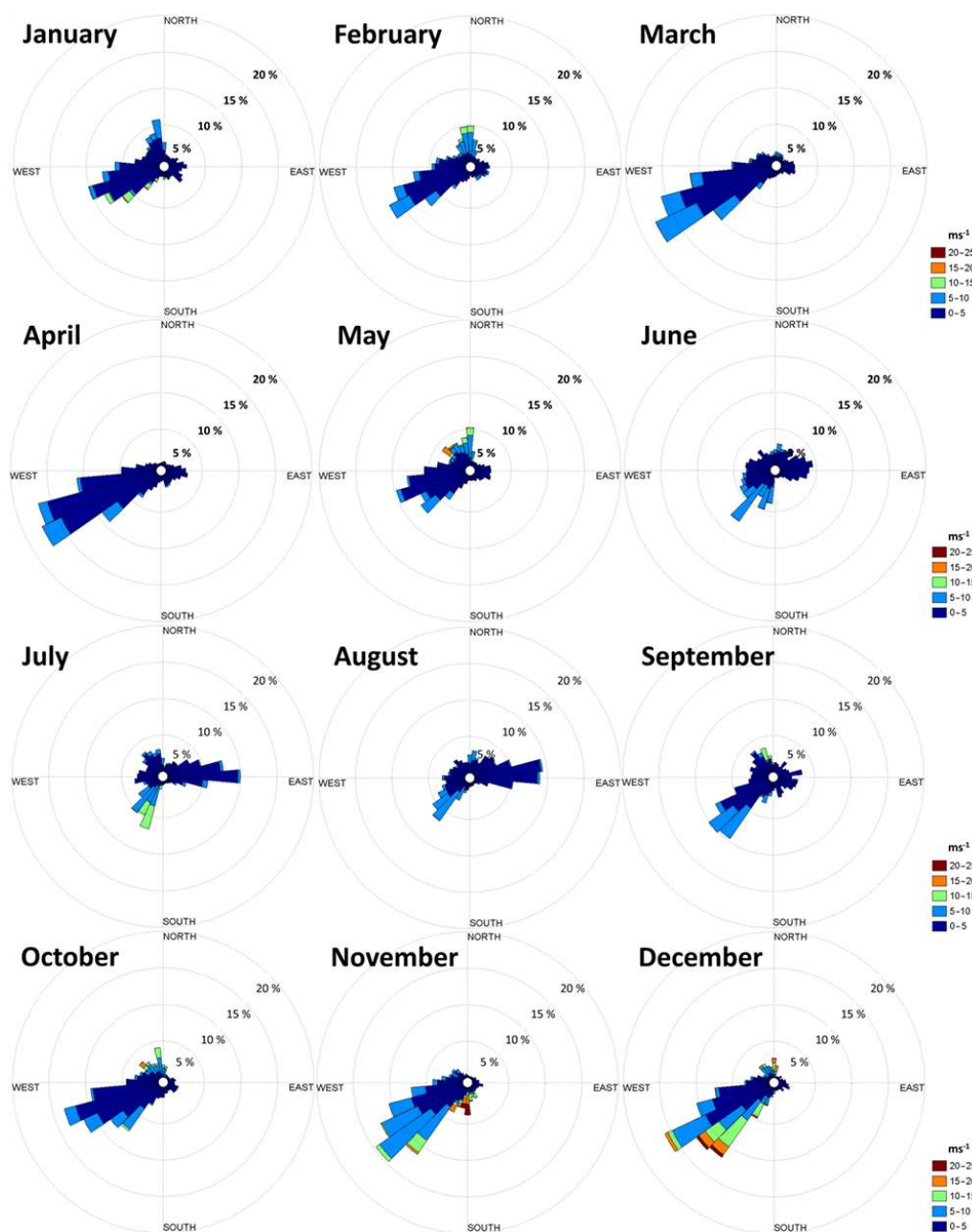


Figure 5. Wind roses showing monthly wind direction and wind speed at Station Nord during 2012. The concentric rings show the percentage of wind arriving from a particular direction.

in the Arctic by Heintzenberg et al. (2015) also showed a strong coupling of newly formed particles and the traveling of air masses over open water. At the same time, it must be noted that wind measurements using the sonic anemometer were confined to local observations at ground level, which according to radio sound measurements by Batchvarova et al. (2013), do not capture activities such as transport of air masses at higher altitudes, or regional transport of air masses. The extent of wind impacts on the particle size distributions at the station is thus not well constrained.

Previous studies reported a dependence of particle number concentrations on wind speed in the Arctic (Leck et al., 2002) and North Atlantic (Odowd and Smith, 1993). However, in this study, the accumulation-mode particles (110–900 nm) only showed positive correlation with wind speed during 8 out of 12 months of 2012, with a moderate Pearson correlation coefficient range of 0.05–0.38. The reason could be partly attributed to the larger size ranges (500 nm up to 16 μm in diameter) measured in the other studies, which are more influenced by wind speed.

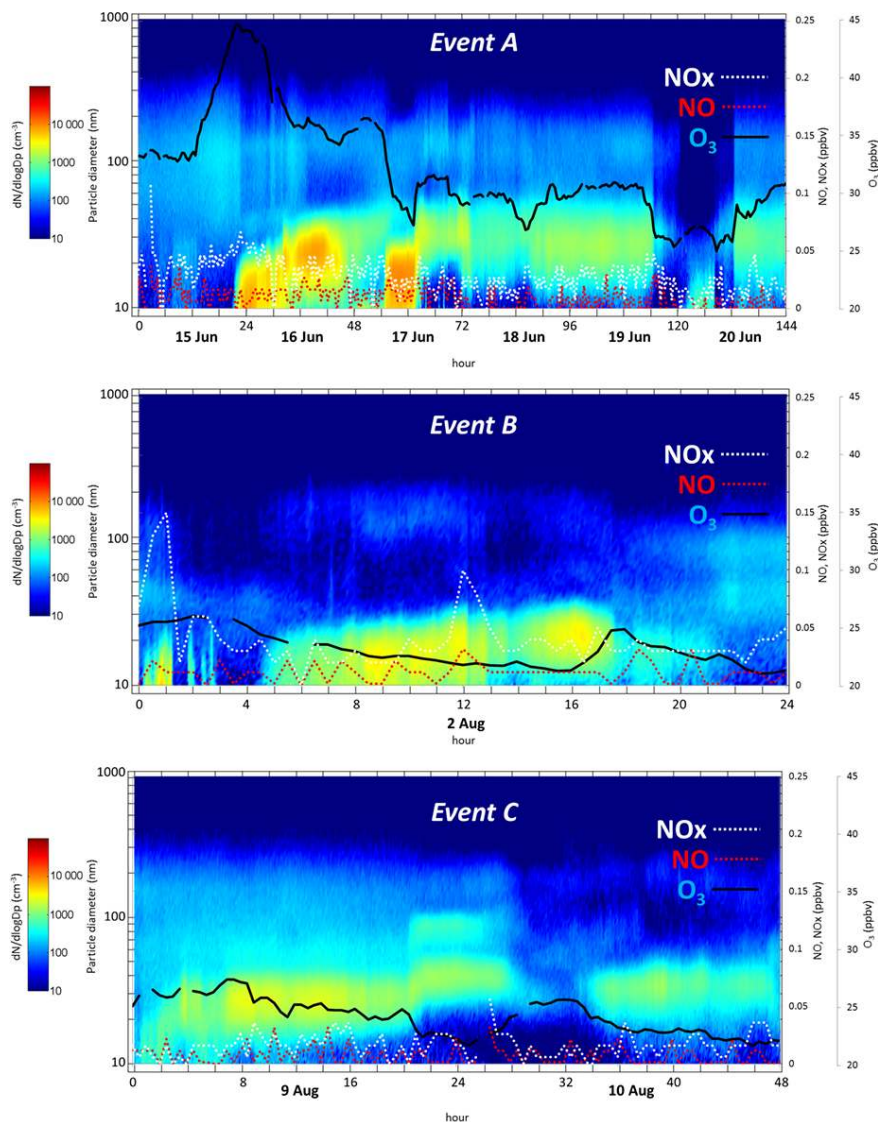


Figure 6. Demonstration of the impacts of O_3 , NO and NO_x on the summer new particle formation events occurring on 15–20 June (Event A), 2 August (Event B) and 9–10 August (Event C) in 2012.

3.2 New particle formation events

3.2.1 Description of exemplary NPF events

NPF events were observed at the station during the sunlit months, especially during the summer months of June–August, though events were also identified during the months with relatively low sunlight, i.e., March and October. The onset of NPF events was observed during various hours of the day (Fig. S1 in the Supplement). Examples of three events are shown in Fig. 6. As apparent from the figure, the events showed clear but slow growth over considerably long periods up to a few days.

3.2.2 The role of atmospheric oxidants

Figure 6 also shows an overlay of O_3 , NO and NO_x on the NPF event plots to allow analysis of the role of atmospheric oxidants during these events.

Ozone

O_3 shows a strong seasonality in the Arctic troposphere, with maximum springtime concentration observed in the free troposphere, which is however poorly understood (Monks, 2000; Law and Stohl, 2007). It has long been indicated that tropospheric O_3 in the Arctic is enriched from intruding stratospheric air masses (Gregory et al., 1992; Gruzdev and Sitnov, 1993). A recent model study has also suggested

that summertime photochemical production of O_3 by NO_x in the Arctic could also be a dominant source (Walker et al., 2012). This was attributed to NO_x emissions from the thermal decomposition of the long-lived reservoir species peroxyacetyl nitrate (PAN) during summer (Fan et al., 1994). Meanwhile, transport from midlatitude source regions could also contribute to the O_3 budget in the Arctic during autumn and winter (Walker et al., 2012). Sources of O_3 in the Arctic could therefore be a combination of different factors, including, among others, stratospheric influence, local production and transport from midlatitude sources. Finally, surface O_3 is also depleted every spring due to reactions with Br atoms released from sea ice and surface snow (Barrie et al., 1988; Simpson et al., 2007; Skov et al., 2004; Bottenheim et al., 1990; Pratt et al., 2013; Abbatt, 2013), similar to O_3 depletion in the stratosphere.

In this work, O_3 was used as a tracer of atmospheric chemical processes, and the concentration of O_3 was found to be related to the formation and growth of new particles at Station Nord during summer based on case studies of NPF events in 2012 (Fig. 6).

Event A, Fig. 6: Event A is in fact a “double” event, with the first event occurring over 15–16 June followed by another event starting on 17 June with traceable growth until 20 June.

During 15 June, the O_3 level (black line) increased considerably to ~ 45 ppbv, which was significantly higher than the average summer (June–August 2012) concentration of O_3 (~ 26 ppbv). As the NPF event on 15 June started followed by particle growth up to ~ 25 nm, the O_3 level dropped dramatically, then somewhat stabilized when the approximate mean particle size reaches the lower Aitken mode. The next drop in O_3 concentration (from ~ 37 to ~ 27 ppbv) coincided with the occurrence of the second NPF event observed around noon on 17 June. As the new particles grew beyond ~ 30 nm in diameter, the O_3 concentration seemed to stabilize again.

In the late hours of 19 June, the O_3 concentration suddenly dropped by ~ 5 ppbv, coinciding with an interruption of the event. By midday on 20 June, the O_3 concentration increased back to the pre-interruption level, while that interrupted event also seemed to be brought back to the station. It was unclear if this drop of O_3 concentration on 19 June was associated with any NPF, as nucleation-sized particles were also observed for a few hours during the early hours of 20 June. However, a full justification of this observation was not possible due to the detection limit of the Mobility Particle Size Spectrometer system (~ 10 nm), confined to only aged nucleation particles. Another explanation could be that both O_3 and the nucleation event were transported to the station from a common source, with the interruption probably indicating, for instance, a displacement of air mass.

During the Event A case study, the NO and NO_x level remained mostly below 0.1 ppbv. This was approximately the background level of NO_x at Station Nord throughout the year. At the same time, it must be noted that this level is be-

low the detection limit of the instrument (150 ppt), and thus must be treated with caution. NO and NO_x concentration did not seem to relate to O_3 concentration level, or observations of new particle formation events.

Event B, Fig. 6: This event on 2 August showed that a lower level of O_3 concentration (~ 25 ppbv) could also be associated with a new particle formation event. During the event, the episode of traceable particle growth lasted for approximately 12 h, coinciding with a concurrent drop of the O_3 concentration. This event was also considerably less intensive in regards of particle number concentrations compared to Event A. Until the end of the event, particles were mostly below 30 nm in size.

Event C, Fig. 6: During this event on 9–10 August, new particle formation was also observed together with lower O_3 concentrations (~ 25 ppbv), which was similar to Event B. The anti-correlation between growth of newly formed particles and O_3 concentration was also observed during this event. However, such anti-correlation was visible until particles almost reached 40–50 nm in diameter, which was higher than that observed during Event A and Event B.

The three events seemed to visually display an anti-correlation between the concentration level of O_3 and the growth trend of smaller particles. A Pearson correlation coefficient between O_3 concentration and integrated particle number concentrations for the nucleation-mode range (10–30 nm) was calculated for each event observed during 2012, where O_3 data were available, and NO_x data were also available to eliminate local pollution spikes. Out of a total of 35 NPF events observed during 2012, 16 events (46 % of total events) displayed a weak to moderate anti-correlation (Pearson correlation coefficient below -0.5) between the integrated particle number concentrations for the nucleation-mode range (10–30 nm) and O_3 , with an average coefficient value of -0.71 . Meanwhile 12 events (34 % of total events) displayed a negative correlation coefficient from -0.05 to -0.41 , with an average value of -0.25 ; and 7 events (20 % of total events) showed a positive correlation in the range of 0.09 to 0.44, with an average value of 0.30. In these later cases (54 % of total events), it can be deemed that there is no relationship between O_3 and the nucleation-mode particle number concentrations. No positive Pearson correlation coefficient stronger than 0.5 was observed.

It is generally agreed that particle nucleation involves sulfuric acid (H_2SO_4) via the oxidation of SO_2 by the hydroxyl (OH) radical (Kulmala et al., 2001), while particle growth depends considerably on vapor uptake and condensation of low-volatile organic vapor products produced by photo-oxidation of volatile organic compounds (VOCs) (Donahue et al., 2011; Riipinen et al., 2011, 2012). Naturally, O_3 is a major atmospheric oxidant, which also undergoes photolysis to form the OH radical oxidant. These oxidants oxidize VOCs to form a variety of low-volatile products. A reduction of O_3 could thus be an indirect indicator of increased availability and thus uptake of low-volatile compounds, contribut-

ing to particle growth. Meanwhile, it should also be noted that the role of halogen chemistry contributing to new particle formation is unknown, due to a lack of relevant data as discussed above.

The source of VOCs at VRS, Station Nord, is unclear. There might be some biogenic emissions of VOCs at the station during summer, expected due to retreated snow and ice cover, exposed bare ground and thus possibly increased biogenic activity. However, since this area is arid, this is expected to be extremely limited. Meanwhile, the presence of VOC oxidation products such as organic acids and organosulfates at the station has been reported by Hansen et al. (2014), though at very low concentrations. The low mass or surface loading of organic materials (Nguyen et al., 2014) and total suspended particles (Nguyen et al., 2013) and thus low condensation sink observed at the station during summer would inhibit removal of small particles by condensation and also coagulation to a lesser extent, thus allowing particle growth and prolonged NPF events. At the same time, no considerable difference in particle mass or surface was observed at the onset of events compared to the average particle mass or surface of the corresponding months during 2012.

NO_x

As mentioned above, sparks of particle formation, which did not grow further, were considered as local pollution events, which were related to NO_x emitted by the car engine during service of the station. There was probably some additional contribution from emissions from the military base, which is located at a distance of about 2.5 km from the measurement site. An example of such interference is illustrated during the early hours of 2 August (Event B, Fig. 6), during which a higher NO_x concentration of ~0.15 ppbv was detected, together with a short episode of new particle formation without further growth. Such interference could also be observed around midday of the same event day (Event B, Fig. 6). In contrast, it must be noted that NO_x concentrations in the range ~0.1–0.2 ppbv were mostly not associated with any noticeable observations of new particle formation. Such episodes with NO_x interference are also demonstrated here as an example and were not included in any calculations of data.

The summer period of June–August was associated with a lower level of background NO_x (NO_x ~0.1 ppbv) compared to the rest of the year (NO_x ~0.2 ppbv). As mentioned above, this low level of background NO_x was mostly below the detection limit of the instrument. NO_x emissions into the Arctic atmosphere other than the direct local anthropogenic emissions could originate from the thermal decomposition of PAN, which is the major atmospheric NO_x reservoir species (Singh et al., 1995). This process is nevertheless limited by low temperature during winter and spring and low PAN levels during summer (Beine and Krognnes, 2000). NO_x also contributes via photochemistry to the local formation of tro-

pospheric O₃, and thus enhances O₃ levels during summer (Walker et al., 2012; Beine and Krognnes, 2000).

3.2.3 Analysis of air mass back trajectories

As mentioned above, the Mobility Particle Size Spectrometer system employed at VRS, Station Nord, is limited to particles larger than 10 nm in size, capturing only aged nucleation particles. It is thus uncertain whether the formation of the freshly nucleated particles actually occurred at the site, or whether they were transported from elsewhere or produced aloft.

Air mass back trajectories were analyzed in order to investigate possible source regions for the observed events. The trajectories were calculated using HYSPLIT (Draxier and Hess, 1998). The model runs were based on meteorological data obtained from the Global Data Assimilation System (GDAS), which is maintained by the US National Centers for Environmental Prediction (NCEP).

In order to facilitate the interpretation of the events shown in Fig. 6, hourly air mass back trajectories were calculated going 72 h backwards for air masses arriving at the station at 50 and 500 m above sea level. The trajectories are presented in Fig. 7, with the names of the events kept consistent with those in Fig. 6. Calculations of air mass back trajectories were performed for 3-day periods, in order to minimize the uncertainties associated with calculating longer trajectories.

As can be seen in Fig. 7, westerly air masses were arriving at the station during the hours before the onset of Event A. At 21:00 on 15 June, air masses started to originate from the southwesterly direction instead, which also marks the observation of the first NPF event. In fact, during both NPF events identified on 15 and 17 June, during Event A, air masses seemed to be fast-moving, originating from longer distances in the southwesterly direction. During the late hours of 17 June to early 19 June, the station started to receive more air masses arriving from a northerly direction (for example 19 June, 06:00 local time), which may associate with the faded nucleation-mode particles observed during this exact time period. The “interrupted period” observed on 19–20 June also seemed to overlap with the time period where air masses were locally confined (for example 19 June, 15:00 local time), and nucleation-mode particles started to be observed again as the air masses started to arrive from a westerly direction instead (20 June, 16:00 local time). It should be noted that this interrupted period was off by about 2 h compared to changes in HYSPLIT air mass trajectories, which might be attributed to uncertainties in HYSPLIT output, especially for calculating air mass movement over small distances in an area with few meteorological measurement data.

The trajectories for Event B (Fig. 7) show that from 05:00 to 18:00 on 2 August, air masses seemed to arrive constantly along the coastline from the northerly direction (which is shown by the example at 06:00, Event B, Fig. 7), compared to the non-event period on that same day, where air masses

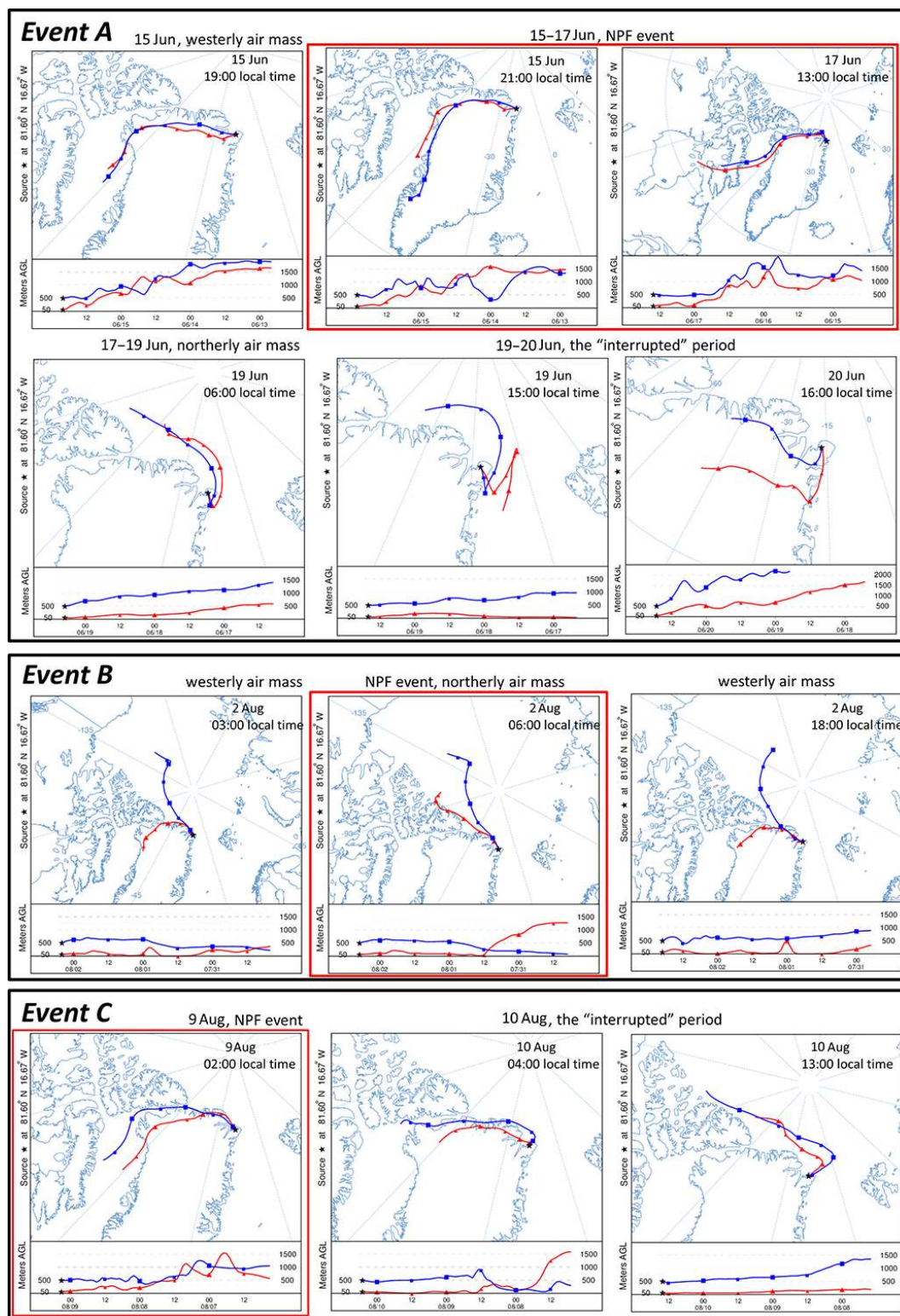


Figure 7. Demonstration of air mass back trajectories calculated hourly using HYSPLIT for arrival at 50 m and 500 m at the station for the case study events.

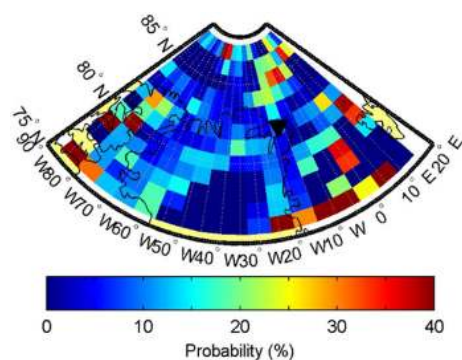


Figure 8. The probability of observing an event at Station Nord (bottom tip of the black triangle) as a function of air mass origin. This figure uses all available data (62 events) from the study period July 2010–February 2013.

were arriving from inland instead (2 August, 03:00 and 18:00 local time). The air masses thus might involve the Arctic sea-ice region (Fig. S2 in the Supplement) and related sources such as open leads or meltwater on top of sea ice due to wind stress as discussed above.

At the same time, the onset of an observed event cannot always be traced using HYSPLIT air mass back trajectories. For example, Event C was observed at the site around 00:00 on 9 August (Fig. 7, Event C) despite no clear changes in HYSPLIT air mass back trajectories. This was a rather weak event which seemed to stem from particle sizes below 10 nm, which were not able to be captured by the Mobility Particle Size Spectrometer. This also highlights the uncertainty with using HYSPLIT to trace the onset of the NPF event, as the onset time might only be for particles above 10 nm in diameter, whereas the air masses transporting particles below 10 nm in size might have arrived at the site prior to this so-called onset time. On the other hand, the interruption of Event C was easier to trace, as it seemed to coincide with the time where the air masses were confined to the inland westerly region prior to arriving at the station (10 August, 04:00 local time). Air mass back trajectories were also calculated 3 days backwards, at 1 h after the starting time of each identified event using HYSPLIT, whereas for the other days, trajectories arriving at 00:00 local time were used. The region around Station Nord was split into 1° latitudinal and 6° longitudinal grid boxes. Every time a trajectory passed one grid box, a count was registered for that grid box. The probability of registering an event, when the air mass originated from a specific grid box, was obtained by dividing the total counts during event days by the sum of total counts during event days, undefined days and non-event days. The probability results are shown in Fig. 8.

As apparent from the figure, the probability of observing an event at the station is low when the air masses arrive from the southwesterly direction over Greenland. Other directions of air mass origin, however, showed relatively similar prob-

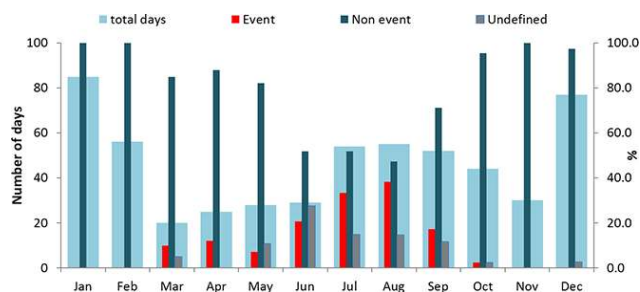


Figure 9. Monthly variation of total number of days with good data (left vertical axis) and frequency percentages (%) of event days, non-event days and undefined days (right vertical axis) during the study period (July 2010–February 2013).

ability of registering an event. A slightly higher probability range was observed for southeasterly air masses that passed over the region, where open waters and melt ponds on ice are more likely to occur. As particles typically grow very slowly at Villum Research Station, the time gap from particle nucleation occurring around 1.5 nm in diameter until the point when they are observed at the site (~ 10 nm in diameter) could range from hours to days. The corresponding probability for observing nucleation-mode particles (~ 10 nm in diameter) at the site should therefore serve as an indication of probable air mass origin of the grown nucleation mode instead of freshly nucleated particles.

3.2.4 Analysis of wind pattern during NPF events

The wind pattern was also investigated on specific event days in 2011 and 2012 (figure not shown). However, these patterns were found to be very similar to the general wind patterns of the corresponding month or period. Therefore, it is unlikely that any change in local wind direction during the specific event days could have an impact on the occurrence of new particle formation events observed at the site. This indicates the possibility of other factors, which may have changed during the event days, affecting new particle formation such as precursors. In fact, Quinn et al. (2002) indicated that the abundant dimethyl sulfide (DMS) could affect particle production during summer, as evidenced by a strong correlation between particle number concentrations and methanesulfonate (MSA^-) concentrations (resulting from the oxidation of DMS). Similar observations were reported by Leitch et al. (2013). Other examples of factors influencing NPF are atmospheric oxidation capacity and transport of air masses.

3.2.5 Event statistics

In general, the event days accounted for 17–38 % of the classified days during June–September, with the highest percentages of event days observed in August (38 %) and July (33 %) (Fig. 9, Table 3). The period from June to early September was also the period during which longer events up to several

Table 3. Percentage of total new particle formation events (marked in blue) vs. non-events and undefined days during the period July 2010 to February 2013. The total events were further divided into class I and class II events. A column of total days (by month) over the studied years was also provided.

	Total days	Class I (%)	Class II (%)	Total events (%)	Non-events (%)	Undefined (%)
January	85	0	0	0	100.0	0
February	56	0	0	0	100.0	0
March	20	0	10.0	10.0	85.0	5.0
April	25	0	12.0	12.0	88.0	0
May	28	0	7.1	7.1	82.1	10.7
June	29	6.9	13.8	20.7	51.7	27.6
July	54	9.3	24.1	33.3	51.9	14.8
August	55	9.1	29.1	38.2	47.3	14.5
September	52	5.8	11.5	17.3	71.2	11.5
October	44	0	2.3	2.3	95.5	2.3
November	30	0	0	0	100.0	0
December	77	0	0	0	97.4	2.6
Total	570	2.6	9.2	11.7	80.8	7.4

days were observed and most class I events were identified (Table 3).

The observed frequencies of event days during these months at VRS, Station Nord, were relatively high compared to reported values from subarctic stations during the same months, such as Värriö (20–25 %) (Kyro et al., 2014), Pallas (10–20 %) (Asmi et al., 2011) or Abisko (< 20 %) (Vaananen et al., 2013), while they overlap with the values of 30–40 % reported by Asmi et al. (2016) from Tiksi, Russian Arctic. In fact, the observed new particle formation events at the subarctic stations and other Nordic stations seemed to show a spring maximum of event occurrence (Vehkamäki et al., 2004; Dal Maso et al., 2007; Kristensson et al., 2008), as opposed to the summer maximum of events observed at VRS, Station Nord. Interestingly, Asmi et al. (2016) found the highest NPF event frequencies in March (50 %), whereas such frequency was only 10 % at VRS, Station Nord, during the same month. It should also be noted that Asmi et al. (2016) reported measuring particle diameters of 7 nm at Tiksi, whereas only those above 10 nm were reported in this study. NPF events were still observed at the subarctic stations Värriö, Pallas and Abisko during the darker months (November–February), though the fraction of event occurrence was typically much lower compared to other seasons (Kyro et al., 2014; Asmi et al., 2011; Väänänen et al., 2013). Notably, not a single event was observed at VRS, Station Nord, during the Arctic night in the absence of sunlight.

4 Conclusion

In this work, the seasonality of particle number size distributions, total particle number, volume and mass concentrations was examined. A strong seasonal pattern was found, showing the abundance of smaller particles during the sunlit

period of the year, especially during summer, and a persistent accumulation mode during the darker months caused by long-range transport of particles to the Arctic. Analysis of wind data showed a dominance of easterly winds during the summer months and southwesterly winds during the darker months of the year.

The observed NPF events at the station lasted from hours to days with various onset times. O₃ was possibly related to the observed NPF events, with 46 % of NPF cases showing a weak to moderate anti-correlation (with an average coefficient value of -0.71) between O₃ concentration and integrated particle number concentrations for the nucleation-mode range (10–30 nm), while no positive correlation was found, and the remainder of events showed no correlation. Calculations of air mass back trajectories on the days with new particle formation events using HYSPLIT indicated that the onset or interruption of events might be explained by changes in air mass origin. Air masses arriving from a southwesterly direction over Greenland were least linked to NPF events, whereas air masses arriving from a southeasterly direction over the Greenland Sea were associated with slightly higher probabilities. Meanwhile, the local wind direction did not seem to relate to NPF events observed at the station.

5 Data availability

The data used in this work were obtained and managed by the Department of Environmental Science at Aarhus University, Denmark, and can be accessed via correspondence to Quynh T. Nguyen (quynh@eng.au.dk).

The Supplement related to this article is available online at doi:10.5194/acp-16-11319-2016-supplement.

Acknowledgements. This work was financially supported by the Danish Environmental Protection Agency with means from the MIKA/DANCEA funds for Environmental Support to the Arctic Region, which is part of the Danish contribution to “Arctic Monitoring and Assessment Program” (AMAP) and to the Danish research project “Short-lived Climate Forcers” (SLCF). The findings and conclusions presented here do not necessarily reflect the views of the Agency. This work was also supported by the Nordic Centre of Excellence Cryosphere–Atmosphere Interactions in a Changing Arctic Climate (CRAICC). The Villum Foundation is acknowledged for funding the construction of Villum Research Station, Station Nord. The authors are also grateful to the staff at Station Nord for their excellent support.

The Royal Danish Air Force is gratefully acknowledged for providing free transport to Station Nord. The authors are also grateful to the staff at Station Nord for their excellent and unwavering support.

Edited by: M. Boy

Reviewed by: two anonymous referees

References

- Abbatt, J.: Arctic snowpack bromine release, *Nat. Geosci.*, 6, 331–332, 2013.
- ACIA (Arctic Climate Impact Assessment): Overview Report, Cambridge University Press, Cambridge, 1042 pp., 2005.
- AMAP: Arctic Monitoring and Assessment Programme (AMAP), The Impact of Black Carbon on Arctic Climate Oslo, 72 pp., available at: <http://www.amap.no/documents/doc/the-impact-of-black-carbon-on-arctic-climate/746> (last access: 8 September 2016), 2011.
- Asmi, E., Kivekäs, N., Kerminen, V.-M., Komppula, M., Hyvärinen, A.-P., Hatakka, J., Viisanen, Y., and Lihavainen, H.: Secondary new particle formation in Northern Finland Pallas site between the years 2000 and 2010, *Atmos. Chem. Phys.*, 11, 12959–12972, doi:10.5194/acp-11-12959-2011, 2011.
- Asmi, E., Kondratyev, V., Brus, D., Laurila, T., Lihavainen, H., Backman, J., Vakkari, V., Aurela, M., Hatakka, J., Viisanen, Y., Uttal, T., Ivakhov, V., and Makshtas, A.: Aerosol size distribution seasonal characteristics measured in Tiksi, Russian Arctic, *Atmos. Chem. Phys.*, 16, 1271–1287, doi:10.5194/acp-16-1271-2016, 2016.
- Barrie, L. A., Bottenheim, J. W., Schnell, R. C., Crutzen, P. J., and Rasmussen, R. A.: Ozone Destruction and Photochemical-Reactions at Polar Sunrise in the Lower Arctic Atmosphere, *Nature*, 334, 138–141, doi:10.1038/334138a0, 1988.
- Batchvarova, E. A., Gryning, S. E., Skov, H., Sørensen, L. L., Kirova, H., and Muenkel, C.: Boundary-layer and air quality study at “Station Nord” in Greenland, 33rd International Technical meeting on air pollution Modelling and its applications, 26–30 August, Miami, Florida, USA, 2013.
- Beine, H. J. and Krognes, T.: The seasonal cycle of peroxyacetyl nitrate (PAN) in the European Arctic, *Atmos. Environ.*, 34, 933–940, doi:10.1016/S1352-2310(99)00288-5, 2000.
- Bennartz, R., Shupe, M. D., Turner, D. D., Walden, V. P., Steffen, K., Cox, C. J., Kulie, M. S., Miller, N. B., and Pettersen, C.: July 2012 Greenland melt extent enhanced by low-level liquid clouds, *Nature*, 496, 83–86, 2013.
- Bond, T. C., Doherty, S. J., Fahey, D. W., Forster, P. M., Berntsen, T., DeAngelo, B. J., Flanner, M. G., Ghan, S., Kärcher, B., Koch, D., Kinne, S., Kondo, Y., Quinn, P. K., Sarofim, M. C., Schultz, M. G., Schulz, M., Venkataraman, C., Zhang, H., Zhang, S., Bellouin, N., Guttikunda, S. K., Hopke, P. K., Jacobson, M. Z., Kaiser, J. W., Klimont, Z., Lohmann, U., Schwarz, J. P., Shindell, D., Storelvmo, T., Warren, S. G., and Zender, C. S.: Bounding the role of black carbon in the climate system: A scientific assessment, *J. Geophys. Res.-Atmos.*, 118, 5380–5552, doi:10.1002/jgrd.50171, 2013.
- Bottenheim, J. W., Barrie, L. A., Atlas, E., Heidt, L. E., Niki, H., Rasmussen, R. A., and Shepson, P. B.: Depletion of Lower Tropospheric Ozone during Arctic Spring – the Polar Sunrise Experiment 1988, *J. Geophys. Res.-Atmos.*, 95, 18555–18568, doi:10.1029/Jd095id11p18555, 1990.
- Covert, D. S., Wiedensohler, A., Aalto, P., Heintzenberg, J., McMurry, P. H., and Leck, C.: Aerosol number size distributions from 3 to 500 nm diameter in the arctic marine boundary layer during summer and autumn, *Tellus B*, 48, 197–212, 1996.
- Dal Maso, M., Kulmala, M., Riipinen, I., Wagner, R., Hussein, T., Aalto, P. P., and Lehtinen, K. E. J.: Formation and growth of fresh atmospheric aerosols: eight years of aerosol size distribution data from SMEAR II, Hyytiälä, Finland, *Boreal Environ. Res.*, 10, 323–336, 2005.
- Dal Maso, M., Sogacheva, L., Aalto, P. P., Riipinen, I., Komppula, M., Tunved, P., Korhonen, L., Suur-Uski, V., Hirsikko, A., Kurten, T., Kerminen, V. M., Lihavainen, H., Viisanen, Y., Hansson, H. C., and Kulmala, M.: Aerosol size distribution measurements at four Nordic field stations: identification, analysis and trajectory analysis of new particle formation bursts, *Tellus B*, 59, 350–361, doi:10.1111/j.1600-0889.2007.00267.x, 2007.
- Donahue, N. M., Trump, E. R., Pierce, J. R., and Riipinen, I.: Theoretical constraints on pure vapor-pressure driven condensation of organics to ultrafine particles, *Geophys. Res. Lett.*, 38, L16801, doi:10.1029/2011gl048115, 2011.
- Draxier, R. R. and Hess, G. D.: An overview of the HYSPLIT_4 modelling system for trajectories, dispersion and deposition, *Aust. Meteorol. Mag.*, 47, 295–308, 1998.
- Fan, S. M., Jacob, D. J., Mauzerall, D. L., Bradshaw, J. D., Sandholm, S. T., Blake, D. R., Singh, H. B., Talbot, R. W., Gregory, G. L., and Sachse, G. W.: Origin of Tropospheric NO_x over Sub-Arctic Eastern Canada in Summer, *J. Geophys. Res.-Atmos.*, 99, 16867–16877, doi:10.1029/94jd01122, 1994.
- Flanner, M. G., Zender, C. S., Randerson, J. T., and Rasch, P. J.: Present-day climate forcing and response from black carbon in snow, *J. Geophys. Res.-Atmos.*, 112, D11202, doi:10.1029/2006jd008003, 2007.
- Flanner, M. G., Zender, C. S., Hess, P. G., Mahowald, N. M., Painter, T. H., Ramanathan, V., and Rasch, P. J.: Springtime warming and reduced snow cover from carbonaceous particles, *Atmos. Chem. Phys.*, 9, 2481–2497, doi:10.5194/acp-9-2481-2009, 2009.
- Gregory, G. L., Anderson, B. E., Warren, L. S., Browell, E. V., Bagwell, D. R., and Hudgins, C. H.: Tropospheric ozone and aerosol observations: The Alaskan Arctic, *J. Geophys. Res.-Atmos.*, 97, 16451–16471, doi:10.1029/91jd01310, 1992.

- Gruzdev, A. N. and Sitnov, S. A.: Tropospheric Ozone Annual Variation and Possible Troposphere-Stratosphere Coupling in the Arctic and Antarctic as Derived from Ozone Soundings at Resolute and Amundsen-Scott Stations, *Tellus B*, 45, 89–98, doi:10.1034/j.1600-0889.1993.t01-1-00001.x, 1993.
- Hansen, A. M. K., Kristensen, K., Nguyen, Q. T., Zare, A., Cozzi, F., Nøjgaard, J. K., Skov, H., Brandt, J., Christensen, J. H., Ström, J., Tunved, P., Krejci, R., and Glasius, M.: Organosulfates and organic acids in Arctic aerosols: speciation, annual variation and concentration levels, *Atmos. Chem. Phys.*, 14, 7807–7823, doi:10.5194/acp-14-7807-2014, 2014.
- Hansen, J. and Nazarenko, L.: Soot climate forcing via snow and ice albedos, *P. Natl. Acad. Sci. USA*, 101, 423–428, doi:10.1073/pnas.2237157100, 2004.
- Heidam, N. Z., Wahlin, P., and Christensen, J. H.: Tropospheric gases and aerosols in northeast Greenland, *J. Atmos. Sci.*, 56, 261–278, doi:10.1175/1520-0469(1999)056<0261:TGAAIN>2.0.CO;2, 1999.
- Heidam, N. Z., Christensen, J., Wahlin, P., and Skov, H.: Arctic atmospheric contaminants in NE Greenland: levels, variations, origins, transport, transformations and trends 1990–2001, *Sci. Total Environ.*, 331, 5–28, doi:10.1016/j.scitotenv.2004.03.033, 2004.
- Heintzenberg, J., Leck, C., and Tunved, P.: Potential source regions and processes of aerosol in the summer Arctic, *Atmos. Chem. Phys.*, 15, 6487–6502, doi:10.5194/acp-15-6487-2015, 2015.
- Hirdman, D., Sodemann, H., Eckhardt, S., Burkhardt, J. F., Jefferson, A., Mefford, T., Quinn, P. K., Sharma, S., Ström, J., and Stohl, A.: Source identification of short-lived air pollutants in the Arctic using statistical analysis of measurement data and particle dispersion model output, *Atmos. Chem. Phys.*, 10, 669–693, doi:10.5194/acp-10-669-2010, 2010.
- IPCC: Climate Change 2013: The Physical Science Basis. Contribution of Working Group I to the Fifth Assessment Report of the Intergovernmental Panel on Climate Change, Cambridge University Press, Cambridge, United Kingdom and New York, NY, USA, 1535 pp., 2013.
- Kahl, J. D. W., Martinez, D. A., Kuhns, H., Davidson, C. I., Jaffrezo, J. L., and Harris, J. M.: Air mass trajectories to Summit, Greenland: A 44-year climatology and some episodic events, *J. Geophys. Res.-Oceans*, 102, 26861–26875, doi:10.1029/97jc00296, 1997.
- Karl, M., Leck, C., Gross, A., and Pirjola, L.: A study of new particle formation in the marine boundary layer over the central Arctic Ocean using a flexible multicomponent aerosol dynamic model, *Tellus B*, 64, 17158, doi:10.3402/Tellusb.V64i0.17158, 2012.
- Karl, M., Leck, C., Coz, E., and Heintzenberg, J.: Marine nanogels as a source of atmospheric nanoparticles in the high Arctic, *Geophys. Res. Lett.*, 40, 3738–3743, doi:10.1002/Grl.50661, 2013.
- Korhonen, H., Carslaw, K. S., Spracklen, D. V., Ridley, D. A., and Strom, J.: A global model study of processes controlling aerosol size distributions in the Arctic spring and summer, *J. Geophys. Res.-Atmos.*, 113, D08211, doi:10.1029/2007jd0009114, 2008.
- Kristensson, A., Dal Maso, M., Swietlicki, E., Hussein, T., Zhou, J., Kerminen, V. M., and Kulmala, M.: Characterization of new particle formation events at a background site in Southern Sweden: relation to air mass history, *Tellus B*, 60, 330–344, doi:10.1111/j.1600-0889.2008.00345.x, 2008.
- Kulmala, M., Dal Maso, M., Makela, J. M., Pirjola, L., Vakeva, M., Aalto, P., Miiikkulainen, P., Hameri, K., and O'Dowd, C. D.: On the formation, growth and composition of nucleation mode particles, *Tellus B*, 53, 479–490, doi:10.1034/j.1600-0889.2001.530411.x, 2001.
- Kwok, R.: Outflow of Arctic Ocean Sea Ice into the Greenland and Barents Seas: 1979–2007, *J. Climate*, 22, 2438–2457, doi:10.1175/2008JCLI2819.1, 2009.
- Kyrö, E.-M., Väänänen, R., Kerminen, V.-M., Virkkula, A., Petäjä, T., Asmi, A., Dal Maso, M., Nieminen, T., Juhola, S., Shcherbinin, A., Riipinen, I., Lehtipalo, K., Keronen, P., Aalto, P. P., Hari, P., and Kulmala, M.: Trends in new particle formation in eastern Lapland, Finland: effect of decreasing sulfur emissions from Kola Peninsula, *Atmos. Chem. Phys.*, 14, 4383–4396, doi:10.5194/acp-14-4383-2014, 2014.
- Law, K. S. and Stohl, A.: Arctic air pollution: Origins and impacts, *Science*, 315, 1537–1540, doi:10.1126/science.1137695, 2007.
- Leaitch, W. R., Sharma, S., Huang, L., Toom-Sauntry, D., Chivulescu, A., Macdonald, A. M., Salzen, K. v., Pierce, J. R., Bertram, A. K., Schroder, J. C., Shantz, N. C., Chang, R. Y. W., and Norman, A. L.: Dimethyl sulfide control of the clean summertime Arctic aerosol and cloud, *Elem. Sci. Anth.*, 1, 000017, doi:10.12952/journal.elementa.000017, 2013.
- Leck, C., Norman, M., Bigg, E. K., and Hillamo, R.: Chemical composition and sources of the high Arctic aerosol relevant for cloud formation, *J. Geophys. Res.-Atmos.*, 107, 4135, doi:10.1029/2001JD001463, 2002.
- Li, S. M. and Barrie, L. A.: Biogenic Sulfur Aerosol in the Arctic Troposphere .1. Contributions to Total Sulfate, *J. Geophys. Res.-Atmos.*, 98, 20613–20622, doi:10.1029/93JD02234, 1993.
- Markus, T., Stroeve, J. C., and Miller, J.: Recent changes in Arctic sea ice melt onset, freezeup, and melt season length, *J. Geophys. Res.-Oceans*, 114, C12024, doi:10.1029/2009jc005436, 2009.
- Massling, A., Nielsen, I. E., Kristensen, D., Christensen, J. H., Sørensen, L. L., Jensen, B., Nguyen, Q. T., Nøjgaard, J. K., Glasius, M., and Skov, H.: Atmospheric black carbon and sulfate concentrations in Northeast Greenland, *Atmos. Chem. Phys.*, 15, 9681–9692, doi:10.5194/acp-15-9681-2015, 2015.
- Middlebrook, A. M., Murphy, D. M., and Thomson, D. S.: Observations of organic material in individual marine particles at Cape Grim during the First Aerosol Characterization Experiment (ACE 1), *J. Geophys. Res.-Atmos.*, 103, 16475–16483, doi:10.1029/97jd03719, 1998.
- Monks, P. S.: A review of the observations and origins of the spring ozone maximum, *Atmos. Environ.*, 34, 3545–3561, doi:10.1016/S1352-2310(00)00129-1, 2000.
- National Snow and Ice Data Center: available at: <http://nsidc.org/>, last access: 19 February 2016.
- Nguyen, Q. T., Skov, H., Sørensen, L. L., Jensen, B. J., Grube, A. G., Massling, A., Glasius, M., and Nøjgaard, J. K.: Source apportionment of particles at Station Nord, North East Greenland during 2008–2010 using COPREM and PMF analysis, *Atmos. Chem. Phys.*, 13, 35–49, doi:10.5194/acp-13-35-2013, 2013.
- Nguyen, Q. T., Kristensen, T. B., Hansen, A. M. K., Skov, H., Bossi, R., Massling, A., Sorensen, L. L., Bilde, M., Glasius, M., and Nøjgaard, J. K.: Characterization of humic-like substances in Arctic aerosols, *J. Geophys. Res.-Atmos.*, 119, 5011–5027, doi:10.1002/2013jd020144, 2014.
- O'Dowd, C. D. and Smith, M. H.: Physicochemical Properties of Aerosols over the Northeast Atlantic – Evidence for Wind-Speed-Related Submicron Sea-Salt Aerosol Production, *J. Geo-*

- phys. Res.-Atmos., 98, 1137–1149, doi:10.1029/92jd02302, 1993.
- Pfeifer, S., Birmili, W., Schladitz, A., Müller, T., Nowak, A., and Wiedensohler, A.: A fast and easy-to-implement inversion algorithm for mobility particle size spectrometers considering particle number size distribution information outside of the detection range, *Atmos. Meas. Tech.*, 7, 95–105, doi:10.5194/amt-7-95-2014, 2014.
- Pirjola, L., O'Dowd, C. D., Brooks, I. M., and Kulmala, M.: Can new particle formation occur in the clean marine boundary layer?, *J. Geophys. Res.-Atmos.*, 105, 26531–26546, doi:10.1029/2000jd900310, 2000.
- Pnyushkov, A. V., Polyakov, I. V., Ivanov, V. V., and Kikuchi, T.: Structure of the Fram Strait branch of the boundary current in the Eurasian Basin of the Arctic Ocean, *Polar Sci.*, 7, 53–71, doi:10.1016/j.polar.2013.02.001, 2013.
- Pratt, K. A., Custard, K. D., Shepson, P. B., Douglas, T. A., Pohler, D., General, S., Zielcke, J., Simpson, W. R., Platt, U., Tanner, D. J., Gregory Huey, L., Carlsen, M., and Stirm, B. H.: Photochemical production of molecular bromine in Arctic surface snowpacks, *Nat. Geosci.*, 6, 351–356, doi:10.1038/ngeo1779, 2013.
- Quinn, P. K., Miller, T. L., Bates, T. S., Ogren, J. A., Andrews, E., and Shaw, G. E.: A 3-year record of simultaneously measured aerosol chemical and optical properties at Barrow, Alaska, *J. Geophys. Res.-Atmos.*, 107, doi:10.1029/2001jd001248, 2002.
- Quinn, P. K., Bates, T. S., Baum, E., Doubleday, N., Fiore, A. M., Flanner, M., Fridlind, A., Garrett, T. J., Koch, D., Menon, S., Shindell, D., Stohl, A., and Warren, S. G.: Short-lived pollutants in the Arctic: their climate impact and possible mitigation strategies, *Atmos. Chem. Phys.*, 8, 1723–1735, doi:10.5194/acp-8-1723-2008, 2008.
- Riipinen, I., Pierce, J. R., Yli-Juuti, T., Nieminen, T., Häkkinen, S., Ehn, M., Junninen, H., Lehtipalo, K., Petäjä, T., Slowik, J., Chang, R., Shantz, N. C., Abbatt, J., Leaitch, W. R., Kerminen, V.-M., Worsnop, D. R., Pandis, S. N., Donahue, N. M., and Kulmala, M.: Organic condensation: a vital link connecting aerosol formation to cloud condensation nuclei (CCN) concentrations, *Atmos. Chem. Phys.*, 11, 3865–3878, doi:10.5194/acp-11-3865-2011, 2011.
- Riipinen, I., Yli-Juuti, T., Pierce, J. R., Petaja, T., Worsnop, D. R., Kulmala, M., and Donahue, N. M.: The contribution of organics to atmospheric nanoparticle growth, *Nat. Geosci.*, 5, 453–458, doi:10.1038/ngeo1499, 2012.
- Sellegri, K., O'Dowd, C. D., Yoon, Y. J., Jennings, S. G., and de Leeuw, G.: Surfactants and submicron sea spray generation, *J. Geophys. Res.-Atmos.*, 111, D22215, doi:10.1029/2005jd006658, 2006.
- Shupe, M. D. and Intrieri, J. M.: Cloud radiative forcing of the Arctic surface: The influence of cloud properties, surface albedo, and solar zenith angle, *J. Climate*, 17, 616–628, doi:10.1175/1520-0442(2004)017<0616:Grfota>2.0.Co;2, 2004.
- Simpson, W. R., von Glasow, R., Riedel, K., Anderson, P., Ariya, P., Bottenheim, J., Burrows, J., Carpenter, L. J., Frieß, U., Goodsite, M. E., Heard, D., Hutterli, M., Jacobi, H.-W., Kaleschke, L., Neff, B., Plane, J., Platt, U., Richter, A., Roscoe, H., Sander, R., Shepson, P., Sodeau, J., Steffen, A., Wagner, T., and Wolff, E.: Halogens and their role in polar boundary-layer ozone depletion, *Atmos. Chem. Phys.*, 7, 4375–4418, doi:10.5194/acp-7-4375-2007, 2007.
- Singh, H. B., Kanakidou, M., Crutzen, P. J., and Jacob, D. J.: High-Concentrations and Photochemical Fate of Oxygenated Hydrocarbons in the Global Troposphere, *Nature*, 378, 50–54, doi:10.1038/378050a0, 1995.
- Skov, H., Christensen, J. H., Goodsite, M. E., Heidam, N. Z., Jensen, B., Wahlin, P., and Geernaert, G.: Fate of elemental mercury in the arctic during atmospheric mercury depletion episodes and the load of atmospheric mercury to the arctic, *Environ. Sci. Technol.*, 38, 2373–2382, doi:10.1021/es030080h, 2004.
- Stendel, M., Christensen, J. H., and Petersen, D.: Arctic climate and climate change with a focus on Greenland, *Adv. Ecol. Res.*, 40, 13–43, doi:10.1016/S0065-2504(07)00002-5, 2008.
- Stroeve, J., Serreze, M., Holland, M., Kay, J., Malanik, J., and Barrett, A.: The Arctic's rapidly shrinking sea ice cover: a research synthesis, *Climatic Change*, 110, 1005–1027, doi:10.1007/s10584-011-0101-1, 2012.
- Ström, J., Umegard, J., Tørseth, K., Tunved, P., Hansson, H. C., Holmen, K., Wismann, V., Herber, A., and König-Langlo, G.: One year of particle size distribution and aerosol chemical composition measurements at the Zeppelin Station, Svalbard, March 2000–March 2001, *Phys. Chem. Earth*, 28, 1181–1190, doi:10.1016/j.pce.2003.08.058, 2003.
- Tervahattu, H., Juhanoja, J., and Kupiainen, K.: Identification of an organic coating on marine aerosol particles by TOF-SIMS, *J. Geophys. Res.-Atmos.*, 107, 4319, doi:10.1029/2001jd001403, 2002.
- Tunved, P., Ström, J., and Krejci, R.: Arctic aerosol life cycle: linking aerosol size distributions observed between 2000 and 2010 with air mass transport and precipitation at Zeppelin station, Ny-Ålesund, Svalbard, *Atmos. Chem. Phys.*, 13, 3643–3660, doi:10.5194/acp-13-3643-2013, 2013.
- Väänänen, R., Kyrö, E.-M., Nieminen, T., Kivekäs, N., Junninen, H., Virkkula, A., Dal Maso, M., Lihavainen, H., Viisanen, Y., Svenningsson, B., Holst, T., Arneth, A., Aalto, P. P., Kulmala, M., and Kerminen, V.-M.: Analysis of particle size distribution changes between three measurement sites in northern Scandinavia, *Atmos. Chem. Phys.*, 13, 11887–11903, doi:10.5194/acp-13-11887-2013, 2013.
- Vehkamäki, H., Dal Maso, M., Hussein, T., Flanagan, R., Hyvärinen, A., Lauros, J., Merikanto, P., Mönkkönen, M., Pihlatie, K., Salminen, K., Sogacheva, L., Thum, T., Ruuskanen, T. M., Keronen, P., Aalto, P. P., Hari, P., Lehtinen, K. E. J., Rannik, Ü., and Kulmala, M.: Atmospheric particle formation events at Värriö measurement station in Finnish Lapland 1998–2002, *Atmos. Chem. Phys.*, 4, 2015–2023, doi:10.5194/acp-4-2015-2004, 2004.
- Walker, T. W., Jones, D. B. A., Parrington, M., Henze, D. K., Murray, L. T., Bottenheim, J. W., Anlauf, K., Worden, J. R., Bowman, K. W., Shim, C., Singh, K., Kopacz, M., Tarasick, D. W., Davies, J., von der Gathen, P., Thompson, A. M., and Carouge, C. C.: Impacts of midlatitude precursor emissions and local photochemistry on ozone abundances in the Arctic, *J. Geophys. Res.-Atmos.*, 117, D01305, doi:10.1029/2011jd016370, 2012.
- Wiedensohler, A., Covert, D. S., Swietlicki, E., Aalto, P., Heintzenberg, J., and Leck, C.: Occurrence of an ultrafine particle mode less than 20 nm in diameter in the marine boundary layer during Arctic summer and autumn, *Tellus B*, 48, 213–222, doi:10.1034/j.1600-0889.1996.t01-1-00006.x, 1996.

- Wiedensohler, A., Birmili, W., Nowak, A., Sonntag, A., Weinhold, K., Merkel, M., Wehner, B., Tuch, T., Pfeifer, S., Fiebig, M., Fjåraa, A. M., Asmi, E., Sellegri, K., Depuy, R., Venzac, H., Villani, P., Laj, P., Aalto, P., Ogren, J. A., Swietlicki, E., Williams, P., Roldin, P., Quincey, P., Hüglin, C., Fierz-Schmidhauser, R., Gysel, M., Weingartner, E., Riccobono, F., Santos, S., Gröning, C., Faloon, K., Beddows, D., Harrison, R., Monahan, C., Jennings, S. G., O'Dowd, C. D., Marinoni, A., Horn, H.-G., Keck, L., Jiang, J., Scheckman, J., McMurry, P. H., Deng, Z., Zhao, C. S., Moerman, M., Henzing, B., de Leeuw, G., Löschau, G., and Bastian, S.: Mobility particle size spectrometers: harmonization of technical standards and data structure to facilitate high quality long-term observations of atmospheric particle number size distributions, *Atmos. Meas. Tech.*, 5, 657–685, doi:10.5194/amt-5-657-2012, 2012.
- Winklmayr, W., Reischl, G. P., Lindner, A. O., and Berner, A.: A New Electromobility Spectrometer for the Measurement of Aerosol Size Distributions in the Size Range from 1 to 1000 Nm, *J. Aerosol. Sci.*, 22, 289–296, 1991.
- Ziemba, L. D., Dibb, J. E., Griffin, R. J., Huey, L. G., and Beckman, P.: Observations of particle growth at a remote, Arctic site, *Atmos. Environ.*, 44, 1649–1657, doi:10.1016/j.atmosenv.2010.01.032, 2010.
- Zwally, H. J., Abdalati, W., Herring, T., Larson, K., Saba, J., and Steffen, K.: Surface melt-induced acceleration of Greenland ice-sheet flow, *Science*, 297, 218–222, doi:10.1126/science.1072708, 2002.